

We are IntechOpen, the world's leading publisher of Open Access books Built by scientists, for scientists

6,900

Open access books available

186,000

International authors and editors

200M

Downloads

Our authors are among the

154

Countries delivered to

TOP 1%

most cited scientists

12.2%

Contributors from top 500 universities



WEB OF SCIENCE™

Selection of our books indexed in the Book Citation Index
in Web of Science™ Core Collection (BKCI)

Interested in publishing with us?
Contact book.department@intechopen.com

Numbers displayed above are based on latest data collected.
For more information visit www.intechopen.com



Analysis of Natural Frequency, Radial Force and Vibration of Induction Motors Fed by PWM Inverter

Takeo Ishikawa

Additional information is available at the end of the chapter

<http://dx.doi.org/10.5772/49950>

1. Introduction

Lately, as engineers have recognized the importance of having a high-quality working place, the effect of the noise and vibration emitted by inverter-fed induction machines has become a subject to study. Economic considerations force to use less active material. Since the encasing is less stiff, the machine becomes more sensitive to vibrations and noise. Less use of iron in the stator not only yields to a weaker structure but also higher field levels, thus causing higher magnetic forces, which yields to increased vibrations. Then the first aim of this work is to reach a wide knowledge how the levels of noise and vibration generated by the induction motor vary under different working conditions.

Electromagnetic noise is generated when the natural frequencies of vibration of induction motors match or are close to the frequencies present in the electromagnetic force spectrum. In order to avoid such noise and vibration, it is necessary to estimate the amplitude of the radial electromagnetic forces as well as the natural frequencies of the structure. For this reason, several papers have been published to analyze the natural frequencies, electromagnetic force, vibration and acoustic noise. For the analysis of the natural frequencies, a lot of papers have analyzed the stator core without winding. However, it is known that it is difficult to estimate the Young's modulus of winding. For the analysis of the radial force, vibration and acoustic noise, several papers have been published (Ishibashi et al., 2003, Shiohata et al., 1998, Munoz et al., 2003). They gave the amplitudes as well as the frequencies of the radial electromagnetic force. However, they mainly treated the case when the slip was 0. Ishibashi et al. did not consider the rotor current (Ishibashi et al., 2003), and Munoz et al. specified stator currents calculated by MATLAB/Simulink as input data not stator voltages (Munoz et al., 2003).

This paper investigates the vibration of induction motors fed by a Pulse Width Modulation (PWM) inverter. First we analyze the natural frequencies of the stator by considering the stator coil, and compare with the measured ones. Next, we analyze the radial electromagnetic force by using two-dimensional (2D) non-linear finite element method (FEM) which is considering the rotor current and is coupled with voltage equations, and discuss the calculated result with the measured vibration velocity. We clarify the influence of slip, the distributed stator winding and the PWM inverter on the radial force. Moreover, it is well known that a random PWM reduces the acoustic noise emitted from an inverter drive motor (Trzynadlowski et al., 1994). Then, we investigate the radial force of the motor fed by two types of random PWM method, namely, a randomized pulse position PWM and a randomized switching frequency PWM.

2. Natural frequencies

2.1. Analysis method of natural frequencies

The mechanical equation for the stator model with the free boundary condition is expressed as

$$[\mathbf{M}]\{\ddot{\mathbf{x}}\} + [\mathbf{K}]\{\mathbf{x}\} = \{\mathbf{0}\} \quad (1)$$

where, $\{\mathbf{x}\}$ is the node displacement, $[\mathbf{M}]$ and $[\mathbf{K}]$ are the global mass matrix and stiffness matrix. In the two-dimensional (2D) case, the plate is assumed to have constant mass density ρ , area A , uniform thickness h , and motion restricted to the $\{x, y\}$ plane. The element mass matrix is expressed as a 6×6 matrix

$$\mathbf{M}^e = \frac{\rho Ah}{12} \begin{bmatrix} 2 & 0 & 1 & 0 & 1 & 0 \\ 0 & 2 & 0 & 1 & 0 & 1 \\ 1 & 0 & 2 & 0 & 1 & 0 \\ 0 & 1 & 0 & 2 & 0 & 1 \\ 1 & 0 & 1 & 0 & 2 & 0 \\ 0 & 1 & 0 & 1 & 0 & 2 \end{bmatrix} \quad (2)$$

The element stiffness matrix for plane strain is given by

$$\mathbf{K}^e = \frac{E}{(1+\nu)(1-2\nu)} \begin{bmatrix} 1-\nu & \nu & 0 \\ \nu & 1-\nu & 0 \\ 0 & 0 & (1-2\nu)/2 \end{bmatrix} \quad (3)$$

where E is Young's modulus and ν is Poisson's ratio.

Equation (1) leads to the eigenvalue problem,

$$([\mathbf{K}] - \omega_i^2 [\mathbf{M}])\{\Phi\}_i = \{\mathbf{0}\} \quad (4)$$

where, $\{\Phi\}_i$ is eigenvector representing the mode shape of the i -th natural angular frequency ω_i . We solve (4) by discretizing the stator into a finite element mesh and using an eigenvalue subroutine utilized in International Mathematics and Statistics Library (IMSL).

In the calculation of natural frequencies using FEM, the most important but unknown constant is Young's modulus of winding which is composed of the enameled wires, insulation films and vanish. Itori et al. has given the equivalent Young's modulus of winding in slot by the experimental investigation (Itori et al., 2002)

$$E = (0.0319S - 1.05) \times 10^9 \text{ [N / m}^2\text{]} \quad (5)$$

where, S is the space factor of winding.

2.2. Experimental motors

This chapter investigates the vibration characteristics of two motors, hereafter K-model and M-model, whose properties and characteristics are as follows. For M-model, 1.5 kW, 200 volt, 50 Hz, 6.8 A, 4 poles, number of stator slots: 36, number of rotor slots: 44, and one slot-pitch skewing, see Fig.1 (Mori et al., 2005, 2005). For K-model, 100 volt, 50 Hz, 4 poles, number of stator slots: 24, number of rotor slots: 34, stator winding: 66 turns, rotor bar: aluminium, and no skewing, see Fig. 2 (IEEJ, 2002).

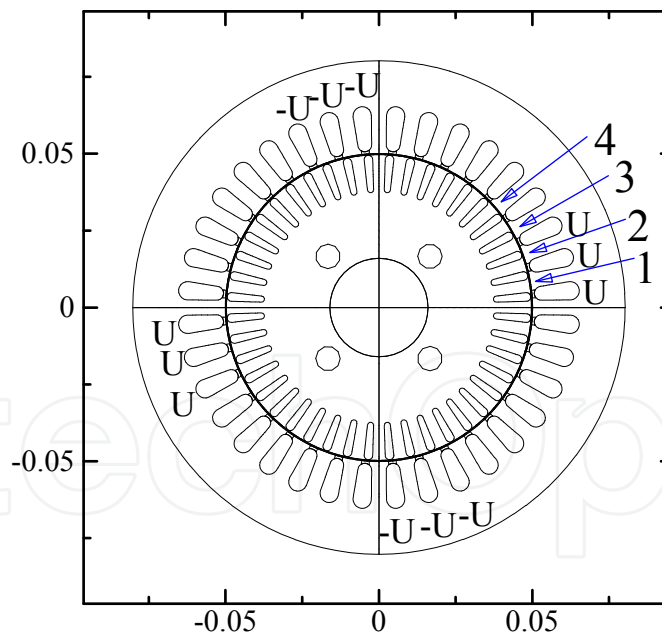


Figure 1. Experimental motor, M-model.

2.3. Measurement of natural frequencies

Natural frequencies are obtained by measuring the transfer function of the stator core. Fig. 3 shows an experimental setup to measure the natural frequencies. A piezoelectric accelerometer PV08A is placed at the top of the stator and is connected to one channel of a

charge amplifier UV-06. An impulse hammer PH-51 is connected to the other channel. The charge amplifier is connected to a signal analyzer SA-01A4, and then to a PC where a software for SA-01A4 is installed.

The transfer function is measured by hammering the stator surface. First, the natural frequencies of the stator core only of M-model are measured. We have removed the stator windings from the stator. Table 1 shows the four lowest measured natural frequencies.

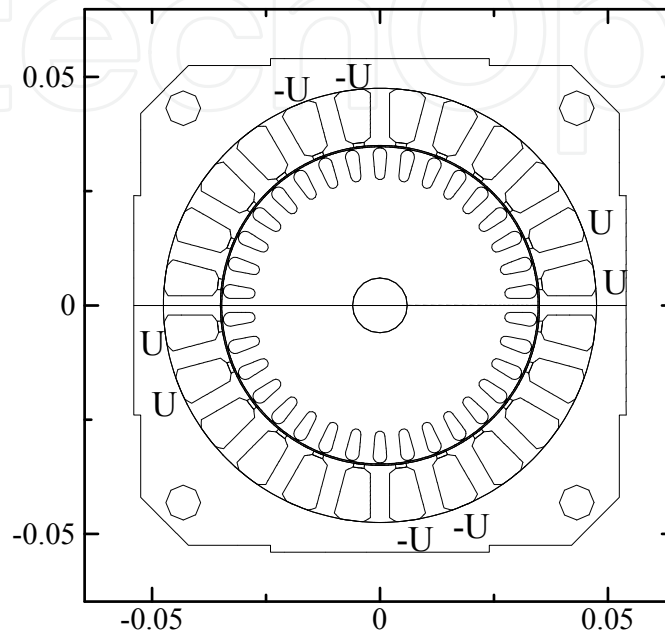


Figure 2. Experimental motor, K-model.

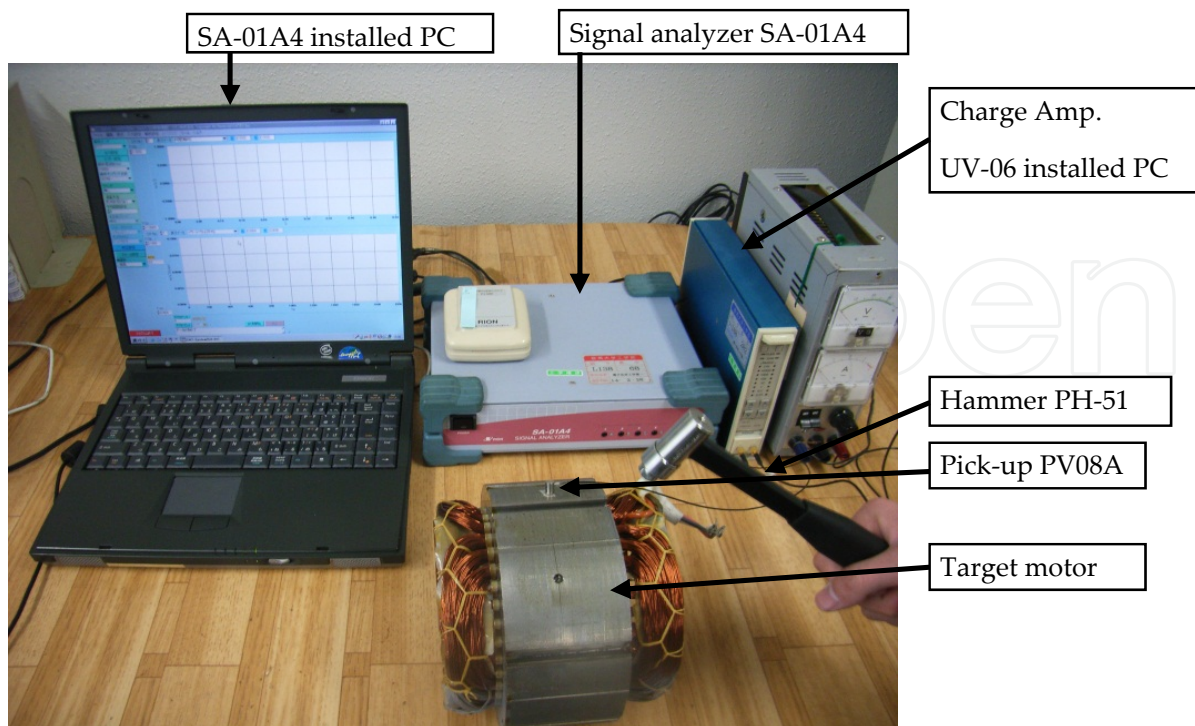


Figure 3. Experimental setup for measurement of natural frequencies.

Mode	Frequency [Hz]
2	1,325
2	1,337
3	3,425
3	3,875

Table 1. Measured natural frequencies of the stator core of M-model motor.

Next, the natural frequencies of the stator with winding of M-model are measured as shown in Fig. 4. The natural frequencies around 1,200Hz are generated from rotor. Three lowest natural frequencies except around 1,200Hz are shown in Table 2.

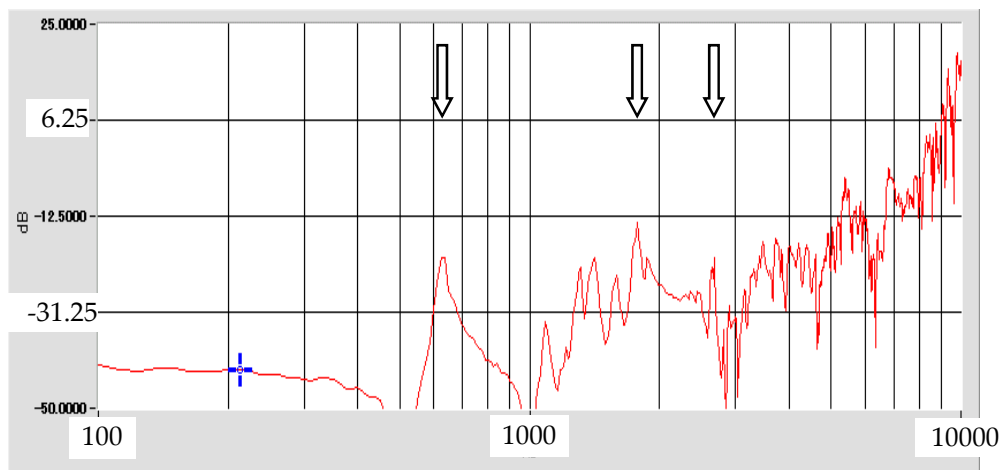


Figure 4. Natural frequencies measured for the whole motor M-model.

Mode	Frequency [Hz]
2	637
3	1,770
4	2,694

Table 2. Three lowest natural frequencies of the M-model motor with stator winding.

2.4. Calculation of natural frequencies

First, we calculate the natural frequencies for the stator core only of the M-model motor, whose mechanical properties include mass density of $7,850\text{kg/m}^3$, Young's modulus of $2.1 \times 10^{10}\text{N/m}^2$ and Poisson's ratio of 0.3. Table 3 shows the comparison of the calculated natural frequencies with the measured ones. It shows a good agreement between the measured values and the calculated ones. In this calculation, we use 18,811 finite element nodes. If we calculate the natural frequencies with a rough mesh, they become higher values. Fig. 5 shows the modes of stator due to each harmonic. The natural frequencies of 1,369 and 1,425Hz have mode 2, and 3,446 and 3,926Hz have mode 3.

Mode	Measured [Hz]	Calculated [Hz]
2	1,325	1,369
2	1,337	1,425
3	3,425	3,446
3	3,875	3,926

Table 3. Comparison of the calculated natural frequencies with the measured ones for the stator core only.

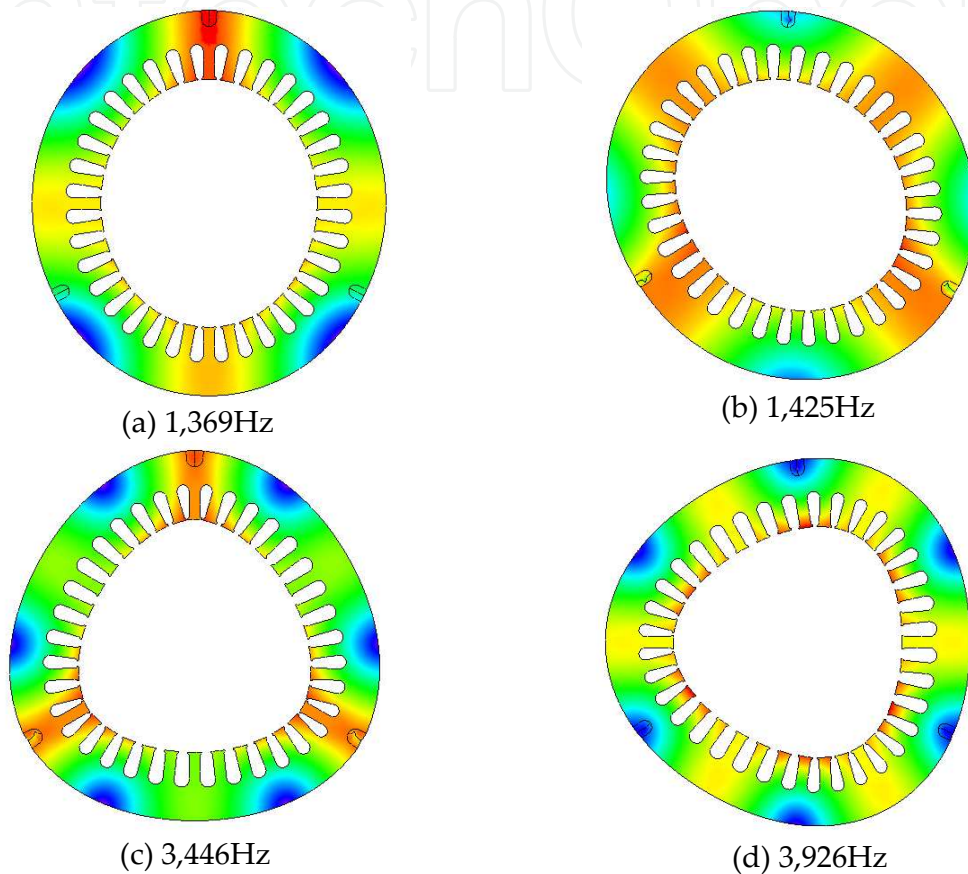


Figure 5. Natural vibration modes for stator core only.

Next, we calculate the natural frequencies of the stator with winding, where the space factor of winding is chosen to be 0.43 by considering the enameled wires. Three lowest natural frequencies and the natural vibration modes are shown in Table 4 and Fig. 6. The natural frequencies of 587, 1,545 and 2,739Hz have mode 2, 3 and 4, respectively.

Mode	Measured [Hz]	Calculated [Hz]
2	637	587.0
3	1,770	1,544.6
4	2,694	2,739.0

Table 4. Comparison of the calculated natural frequencies with the measured ones for the stator with winding.

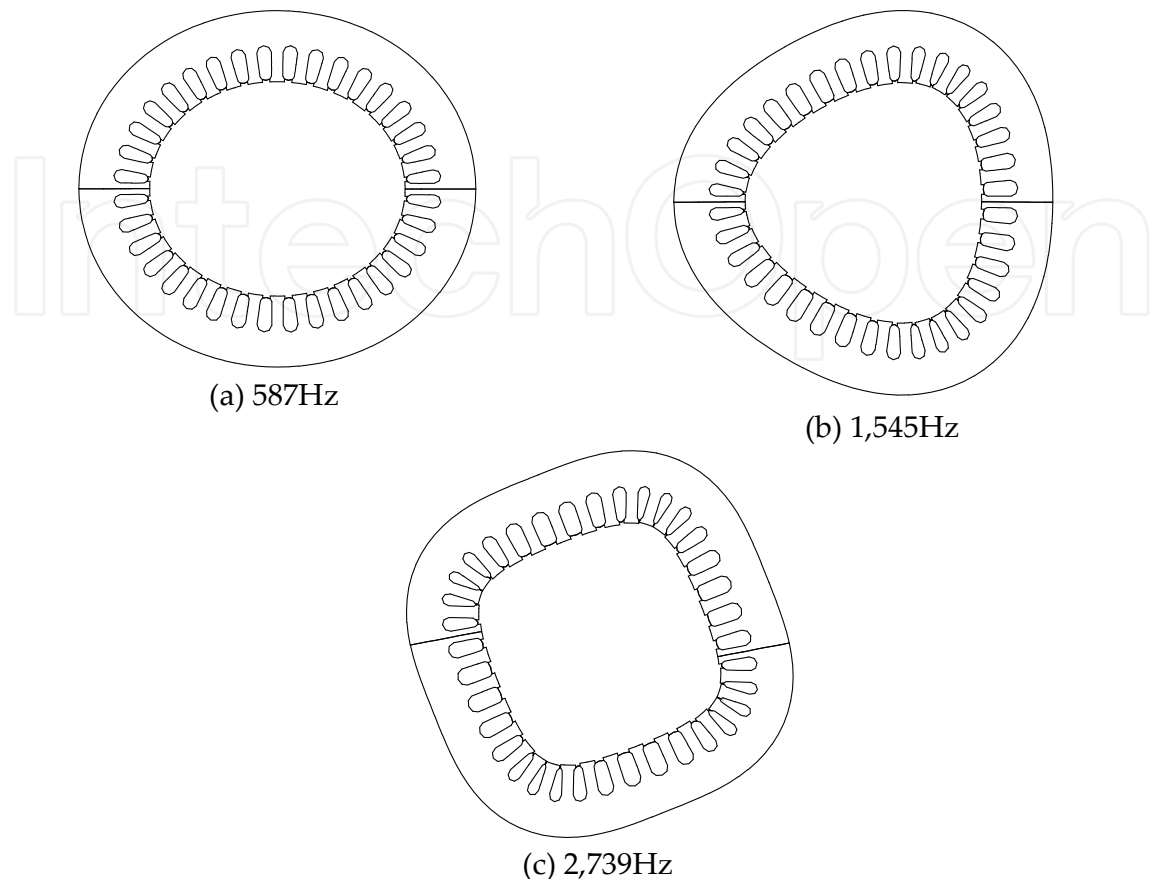


Figure 6. Natural vibration modes for stator with winding.

As the natural frequencies around 1,200Hz are generated from rotor. Three smallest natural frequencies except around 1,200Hz are shown in Table 4 as well as the measured ones. It is shown that the calculated natural frequencies are a little smaller than the measured ones. This is because we calculate the space factor of winding composed of the enameled wires only. If the insulation films and varnish are taken into account, the space factor is larger. Fig. 7 shows the lowest natural frequency by changing the space factor. Therefore, if the insulation films and varnish are taken into account, the smallest natural frequency becomes large, that is, close to the measured one.

3. Radial magnetic force

3.1. Analysis method of radial magnetic force

The simulation of the electromagnetic force is implemented by using a 2D non-linear finite element method considering the rotor current coupled with voltage equations. As we consider the force and vibration at a steady state, the rotating speed is assumed to be constant. Then, the governing equations are as follows,

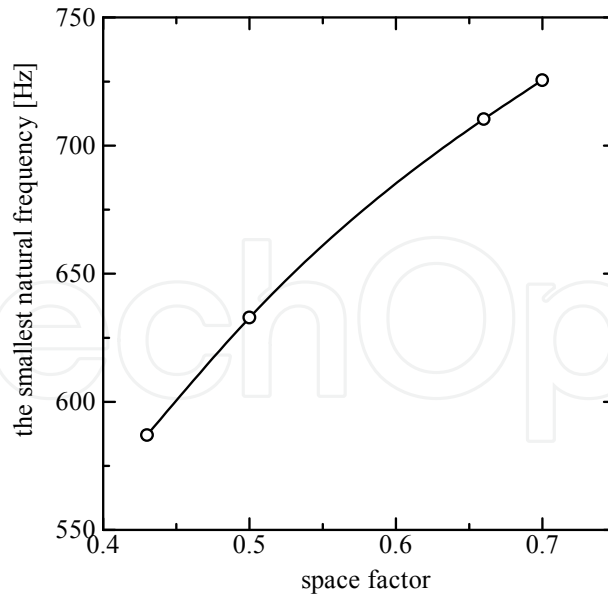


Figure 7. Relationship between the smallest natural frequency and space factor.

$$\frac{\partial}{\partial x} \left(\nu \frac{\partial A}{\partial x} \right) + \frac{\partial}{\partial y} \left(\nu \frac{\partial A}{\partial y} \right) = - \sum_k J_{0k} + \sigma \frac{\partial A}{\partial t} , \quad (6)$$

$$V_k = r i_k + l \frac{d i_k}{d t} + \frac{d \Phi_k}{d t} , \quad (k = a, b, c) \quad (7)$$

$$\text{where } \Phi_k = \frac{n}{S_k} \iint_{S_k} AL \, dx dy , \quad J_{0k} = \frac{n}{S_k} i_k , \quad (8)$$

where, $A, \nu, J_0, \sigma, V, i, r, l, \Phi, n, S, L$ are magnetic vector potential, reluctivity, current density, conductivity, stator phase voltage, stator current, resistance of the stator winding, leakage inductance of the stator end winding, flux linkage, number of turns of stator winding, cross section area of the stator winding, and stack length, respectively. We solve equations (6) and (7) by using the time-stepping FEM. In the case where the motor is driven by the line voltage, the time step Δt is constant so that the step of rotation $\Delta \theta$ is about $2\pi/500$ at slip=0. In the case of PWM inverter, Δt is calculated from the intersection point of a sine wave and a jagged wave with a carrier frequency of 5 kHz. The transient state converged at about five cycles of the input voltage on our simulation. The radial electromagnetic force is calculated by the Maxwell's stress tensor method,

$$F_n = \frac{1}{2\mu_0} (B_n^2 - B_t^2) \quad (9)$$

where, μ_0 is the permeability of air, B_n and B_t are the normal and tangential component of the flux density in the air gap. In order to take into account the 3D effects, the resistance of the end ring of the rotor is considered in the 2D model by modifying the conductivity of the rotor bars. Resistances of bar and end ring can be written as

$$R_b = \frac{1}{\sigma} \frac{l_b}{S_b}$$

$$R_r = \frac{2}{\sigma} \frac{l_r}{S_r} \frac{N_2}{(p\pi)}$$
(10)

where, σ , l_b , S_b , l_r , S_r , N_2 , and p are the conductivity of aluminium, the longitude of the rotor bar, the cross section area of rotor bar, the longitude of the end ring, the cross section area of end ring, the number of rotor slots, and the number of poles, respectively. It is assumed that the rotor resistance is expressed by an equivalent bar with a modified conductivity

$$R_b' = \frac{1}{\sigma'} \frac{l_b}{S_b} = R_b + R_r$$
(11)

Therefore, the modified conductivity is obtained by using the next formula (IEE Japan, 2000)

$$\sigma' = \frac{\frac{l_b}{S_b}}{\frac{l_b}{S_b} + 2 \times \frac{l_r}{S_r} \times \frac{N_2}{(p\pi)^2}} \sigma$$
(12)

Stator end leakage inductance l is also taken into account and given by a traditional method (Horii, 1978)

$$l = \frac{2.3}{2\pi} \mu_0 N^2 l_f \left(\log_{10} \frac{l_f}{d_s} - 0.5 \right)$$
(13)

where, N , l_f , and d_s are number of stator windings, total length of coil end, and diameter of an equivalent circle whose area equals to the cross section of stator coils. If the motor has skewed slots, we should use one of the multi-slice model, the coupled method of 2D and 3D models (Yamasaki, 1996) and the full 3D model (Kometani et al., 1996). The influence that the skewing has on the radial force and vibration is not taken into account in this paper.

3.2. Steady state characteristics

Electromagnetic force is calculated by the 2D non-linear finite element method coupled with voltage equations. The models are created using a triangular mesh with 13,665 elements and 6,907 nodes for the M-model see Fig. 8. One fourth of the motor is calculated because of symmetry. For the M-model these numbers are 14,498 elements and 7,333 nodes, and half of the motor is calculated, see Fig. 9. The values obtained for the aluminium relative conductivity are $\sigma' = 0.737\sigma$ for the K-model, and $\sigma' = 0.351\sigma$ for the M-model.

To corroborate the validity of the model, the measured and calculated values of the output torque and current are compared, and the results are presented in Figs. 10 and 11. The

graphic shows a good agreement between the measured values and the calculated values for both models. This paper does not consider the effect of skewing, then this produces some error around 1400min^{-1} rotating speed in the M-model.

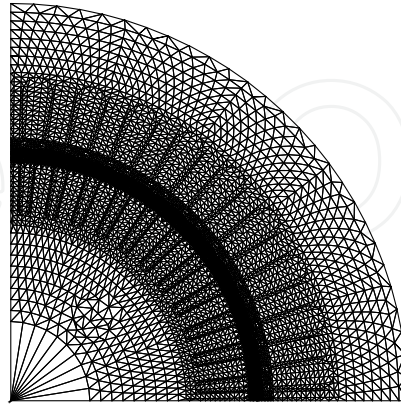


Figure 8. Mesh partition for M-model motor

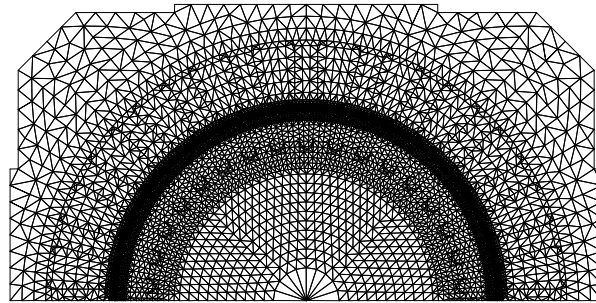


Figure 9. Mesh partition for K-model motor

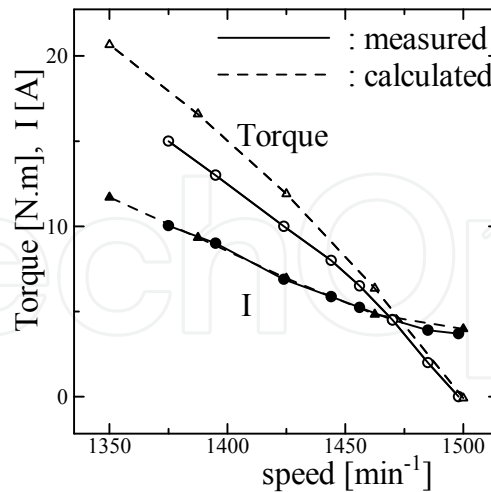


Figure 10. Steady state characteristic for M-model motor

3.3. Radial magnetic force under line source

The space variation of the radial electromagnetic force is presented in Fig. 12. It is shown that the radial force is big at the position where the flux density is big as shown in Fig. 13,

and is approximately flat in the teeth and becomes a small value at the positions where the rotor slot exists.

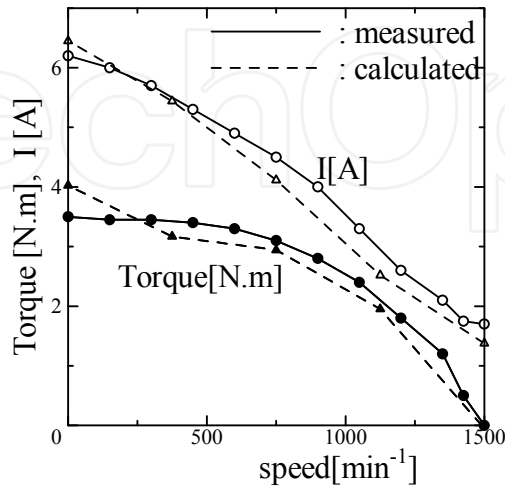


Figure 11. Steady state characteristic for K-model motor

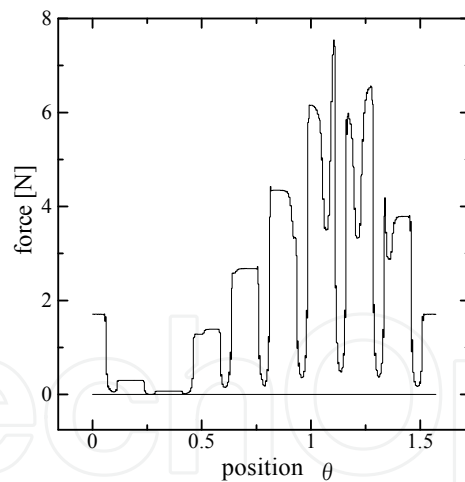


Figure 12. Space variation of radial force.

Fig. 14 shows the time variation of the force at the different teeth. It is shown that the force at tooth 1 is the same as that at tooth 4 and is bigger than those at teeth 2 and 3, because the stator winding is distributed in three slots as shown in Fig. 1.

Figs. 15 and 16 show the radial force and its spectrum at slip=0. It is shown that the force at the teeth is bigger than that at the slots and has a fundamental frequency of 2 times the line frequency of 50Hz. Figs. 17 and 18 show the radial force and its spectrum at slip=0.05. It is shown that the radial force at the slip of 0.05 is very different from that at 0.

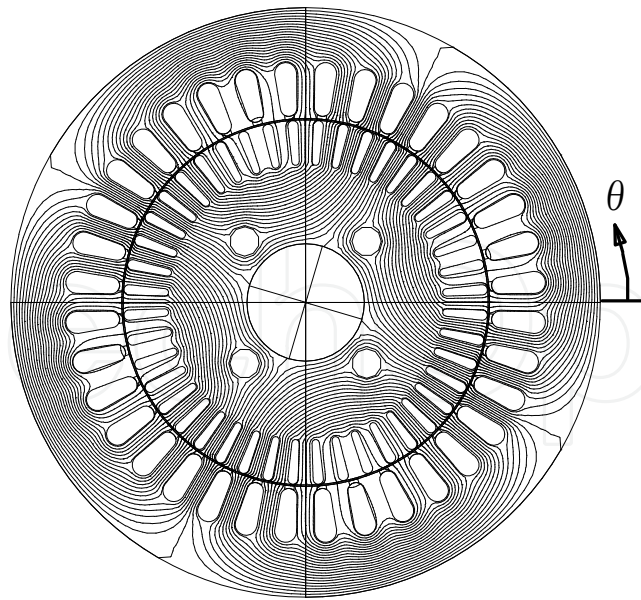


Figure 13. Flux distribution at slip=0.

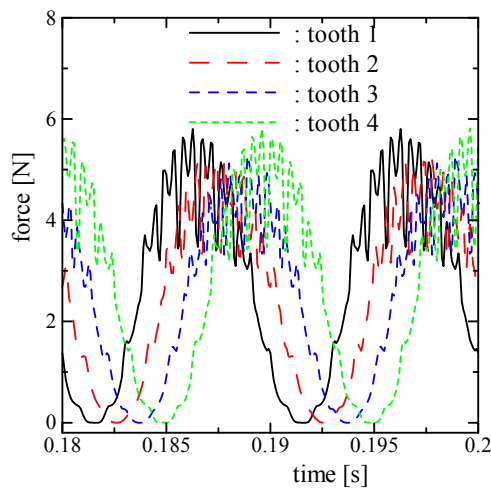


Figure 14. Radial magnetic force at different teeth.

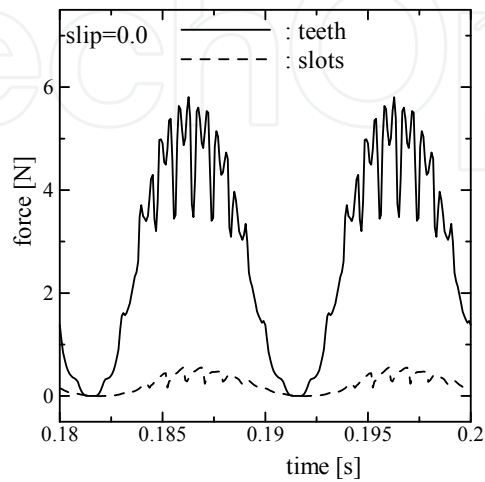


Figure 15. Waveform of radial magnetic force of M model motor at slip=0.

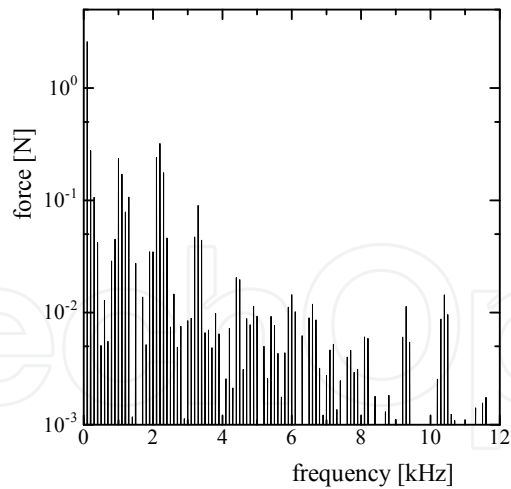


Figure 16. Spectrum of radial magnetic force of M model motor at slip=0.

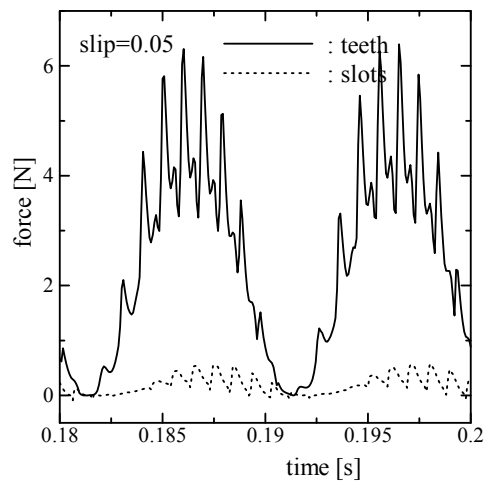


Figure 17. Waveform of radial magnetic force of M model motor at slip=0.05.

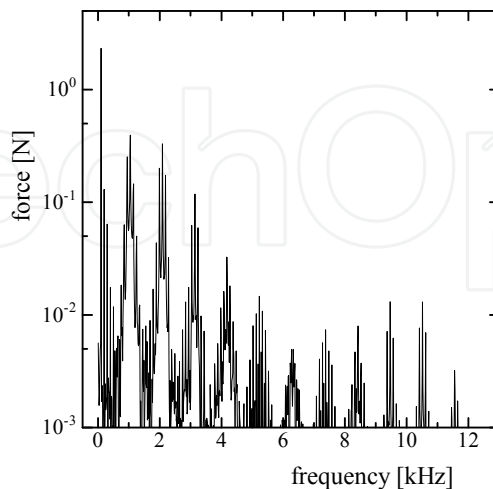


Figure 18. Spectrum of radial magnetic force of M model motor at slip=0.05.

Here we discuss the frequencies of radial force. The electromagnetic flux harmonics are produced due to the relative movement between the rotor and stator. Seeing it from the

stator's side where the main flux is generated, the permeance varies periodically due to the presence of the slots in the rotor. Following this reason, the frequency of the harmonics in the electromagnetic flux is obtained by the product of the fundamental stator magnetomotive force (MMF) and the rotor slot permeance. The fundamental stator MMF F is proportional to $\cos(p/2 \cdot \theta - 2\pi ft)$, where θ is the stator angle. The permeance P is proportional to $1 + \sum A_k \cos kN_2 \left(\theta - \frac{2}{p}(1-s)2\pi ft \right)$, where N_2 , s and k are the number of rotor slots, slip and the order of space harmonics, respectively. Considering that the radial electromagnetic force is proportional to $(F \cdot P)^2$, the next three frequencies are obtained,

$$2f, \frac{2kN_2}{p}(1-s)f, \frac{2kN_2}{p}(1-s)f \pm 2f \quad (14)$$

Since the rotor has 44 slots, when slip is 0, the combination of the slot permeance and the fundamental stator MMF produces the peaks at 100, {1000, 1100, 1200}, {2100, 2200, 2300}, and so on, see Fig. 16. When the slip is 0.05, the frequencies are 100, {945, 1045, 1145}, {1190, 2090, 2190}, see Fig. 18.

In the vibration problems, small space harmonics, namely, small modes are important. Then, we calculate the space and time spectrum of the radial electromagnetic force in the air gap, and show the time spectrum for several space harmonics in Figs. 19 and 20. It is shown that time harmonics of mode 4 are 100, 200, 400, and so on, and the mode of harmonics of 300, 600 and 900Hz is 12.

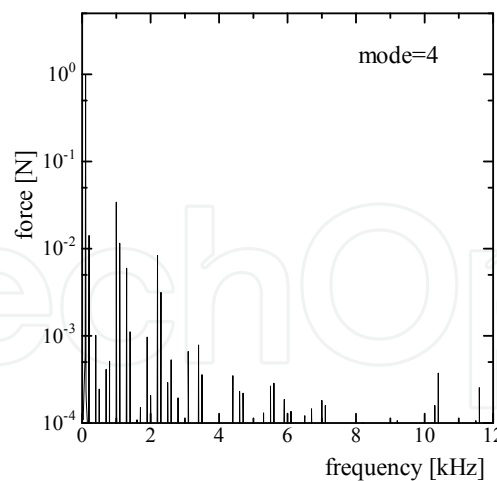


Figure 19. Frequency spectrum for different mode.

For the K-model the rotor has 34 slots, when slip is 0, the combination of the slot permeance and the fundamental stator MMF produces the peaks at 100, {750, 850, 950}, {1600, 1700, 1800}, {2450, 2550, 2650}, and so on, see Fig. 21. When the slip is 0.5, the frequencies are 100, {325, 425, 525}, {750, 850, 950}, see Fig. 22. When slip=1.0, only the first frequency remains and this is appreciated in Fig. 23.

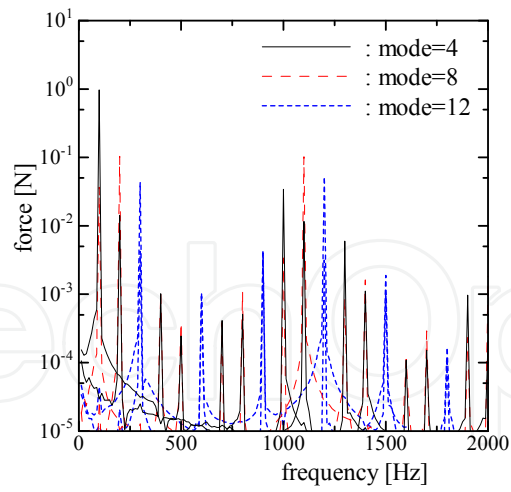


Figure 20. Enlarged one of Fig. 19.

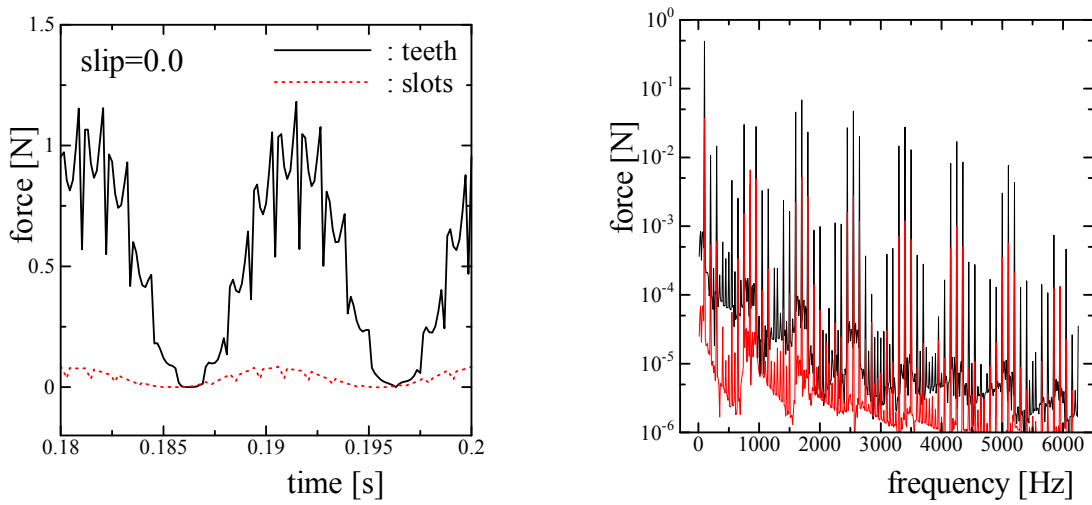


Figure 21. Radial force and its spectrum of K model motor at slip=0.

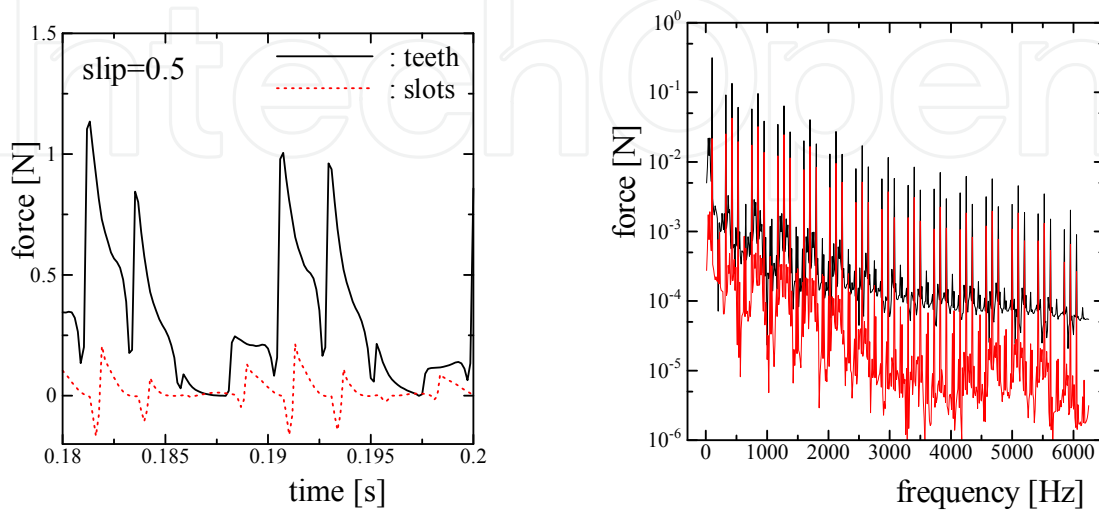


Figure 22. Radial force and its spectrum of K model motor at slip=0.5.

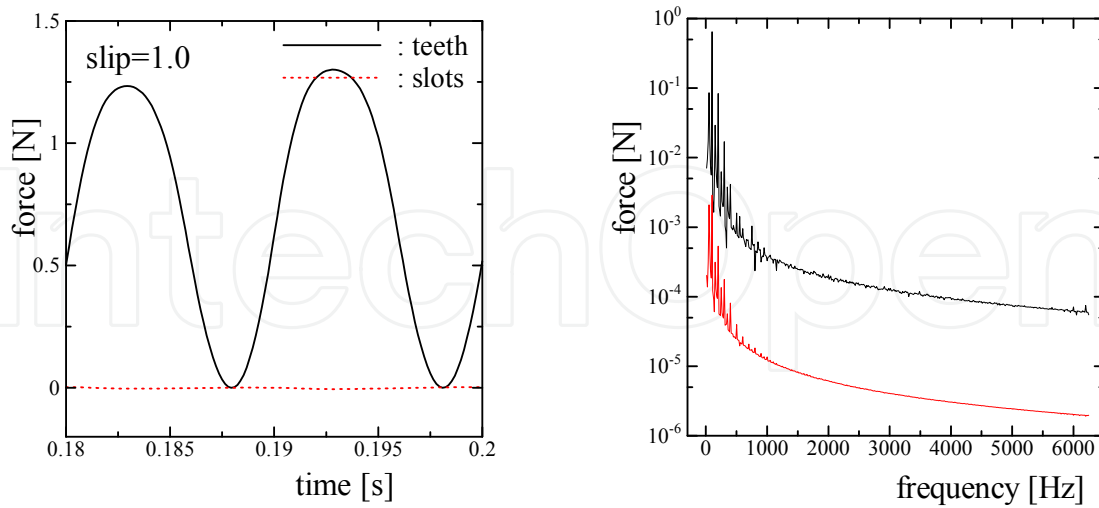


Figure 23. Radial force and its spectrum of K model motor at slip=1.00.

3.4. Radial magnetic force under PWM inverter source

Next, to clarify the difference between the line source and the PWM inverter, Figs. 24 and 25 show the waveforms of torque and stator current at slip=0 and 0.5 for the K-model. The PWM inverter has a carrier frequency of 5kHz and the fundamental amplitude is equal to the line source. It is shown that the current and torque contain the component of the carrier frequency.

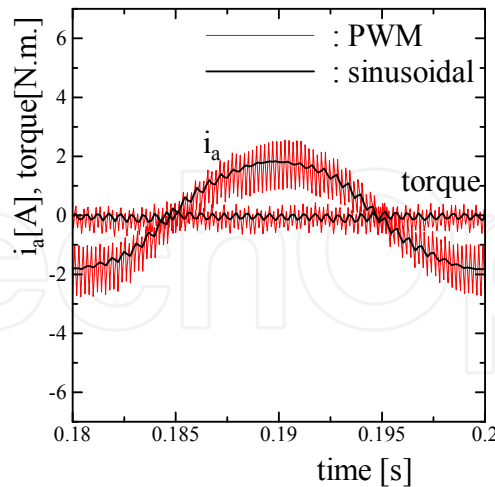


Figure 24. Torque and stator current waveforms of K model driven by PWM inverter, slip=0.

Fig. 26 shows the radial force and its spectrum at slip=0.5 for the K-model. The waveform of radial force driven by the PWM inverter is approximately the same as that driven by the line source. We can find a small noise in the waveform, and find that the amplitude around 5 kHz, that is, carrier frequency is bigger than that of the line source in the spectrum.

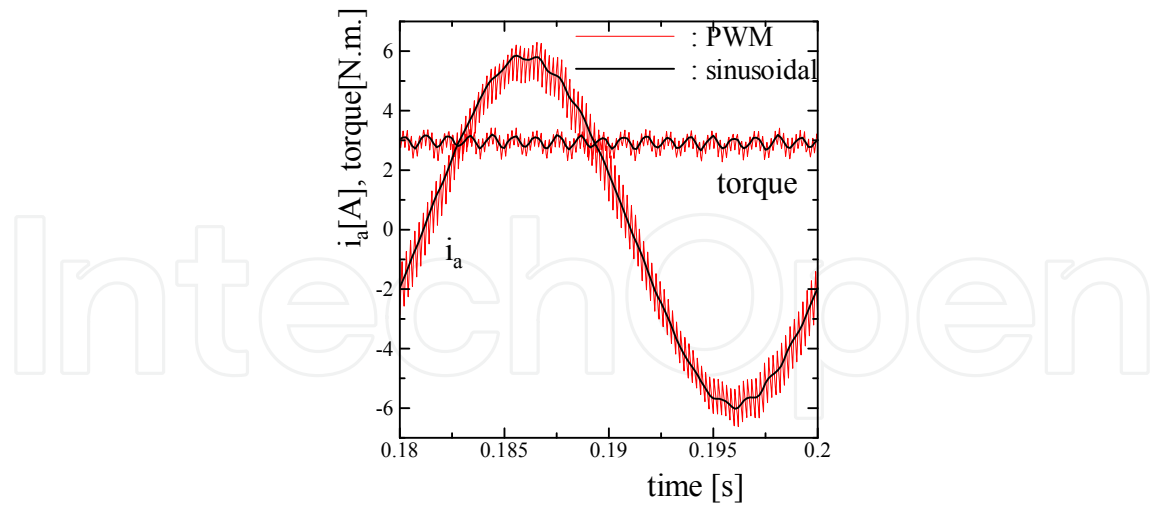


Figure 25. Torque and stator current waveforms of K model driven by PWM inverter, slip=0.5

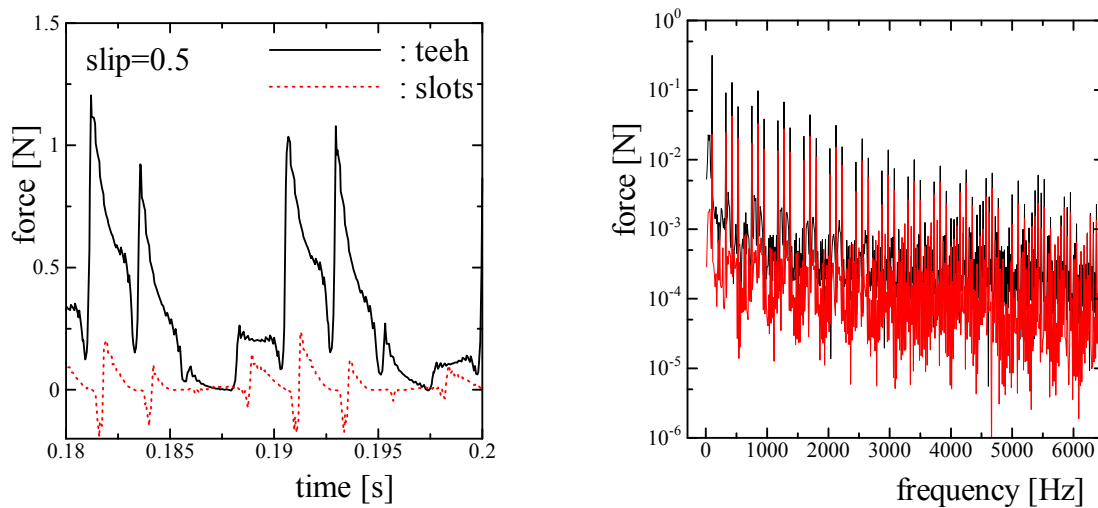


Figure 26. Radial force and frequency spectrum of K-model driven by PWM inverter at slip = 0.5.

3.5. Vibration velocity

Fig. 27 shows the vibration velocity measured at the centre of stator surface, when the motor is running at no-load. The vibration of 600 through 650 Hz is mainly emitted from the natural frequency, and 100, 200, 400, 500, 700, 1000 and 1200 Hz are corresponding to the frequency of the radial force with mode 4. We think that the vibration of 25Hz is emitted by the eccentricity of the rotor. Fig. 28 shows the vibration velocity emitted from the inverter-fed induction motor. We can see the vibration at around nf_c , where n is an integer and f_c is the carrier frequency.

3.6. Radial magnetic force under randomized PWM inverter source

It is well known that a random PWM method reduces the acoustic noise emitted from an inverter drive motor. Then, we analyze the radial force of the motor fed by two types of

random PWM method, namely, a randomized pulse position PWM and a randomized switching frequency PWM. The randomized pulse position PWM changes the pulse width as

$$duty = \frac{v + V_{\max}}{2V_{\max}} + (x - 0.5) * k \quad (15)$$

where, v, V_{\max}, x and k are the voltage reference, the amplitude of the jagged wave with 5 kHz carrier frequency, a random number and the maximum variation of pulse position, respectively. This means that the interval of switching signals is changed by DT , where $-0.5k / 5000 < DT < 0.5k / 5000$ [sec]. The randomized switching frequency PWM changes the switching frequency as

$$f_c = 5000 + (x - 0.5) * (\alpha - 1) * 50 \quad (16)$$

Fig. 29 shows the time spectrum of the radial force of the motor fed by the randomized pulse position PWM, where the end of the interval of switching signals is changed by DT , $-0.2 / 5000 < DT < 0.2 / 5000$ [sec]. Fig. 30 shows the time spectrum by the randomized switching frequency PWM, where the switching frequency is change by DF , $-500 < DF < 500$ [Hz]. The time spectrum shown in Figs 29 and 30 are approximately the same as that under line source, except for the reduction of radial forces at around nf_c . The reduction of radial forces is summarized in Tables 5 and 6.

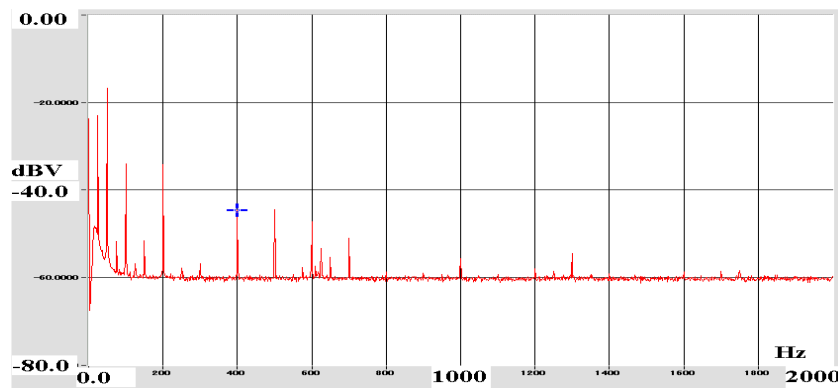


Figure 27. Vibration velocity emitted from M model driven by the line source (measured)

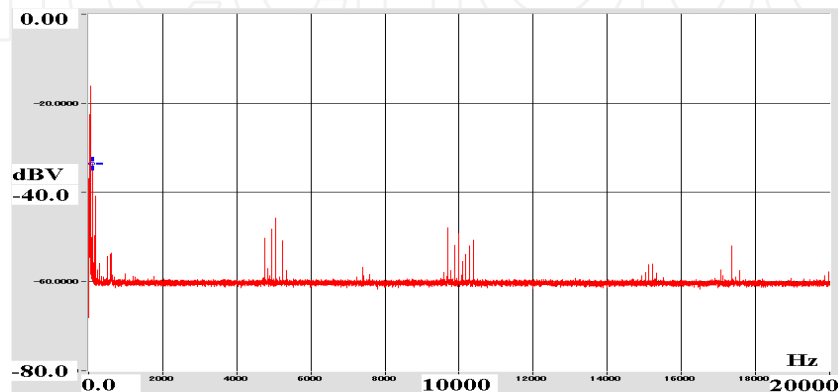


Figure 28. Vibration velocity emitted from M model driven by the PWM inverter source (measured)

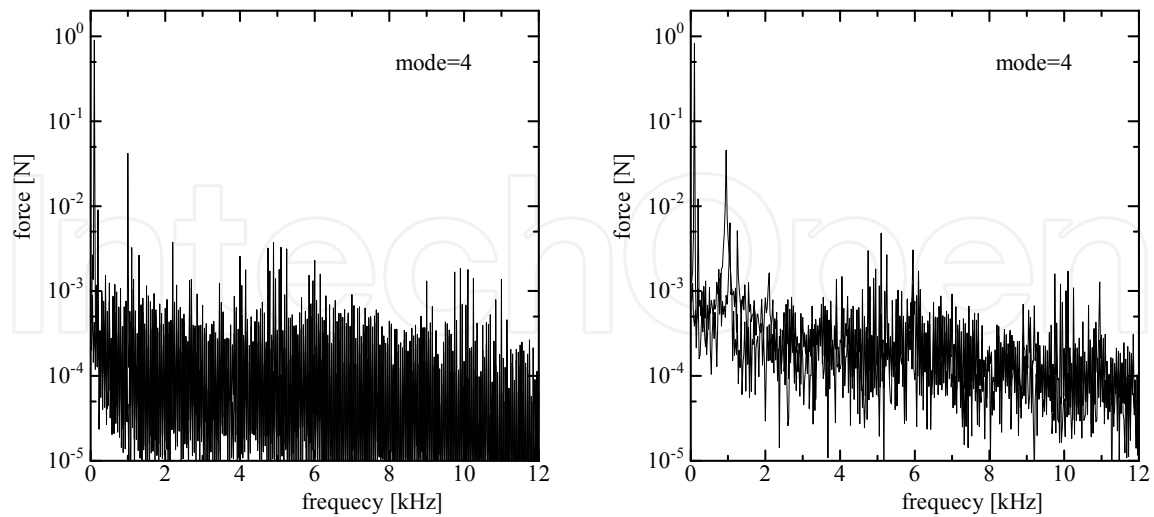


Figure 29. Spectrum of radial force for the randomized pulse position PWM.

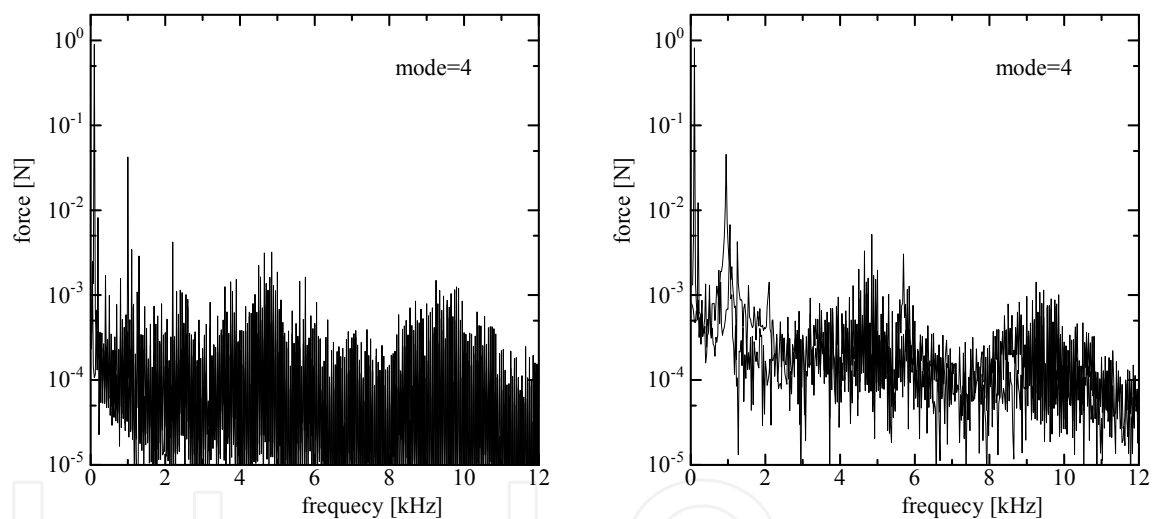


Figure 30. Spectrum of radial force spectrum for the randomized switching frequency PWM.

Frequency	100Hz	400Hz	f_c	$2 f_c$
Line	0.897	0.0437	--	--
PWM	0.896	0.0423	0.00366	0.00260
P PWM	0.904	0.0418	0.00375	0.00185
F PWM	0.899	0.0423	0.00321	0.00125

P PWM: Randomized pulse position PWM,
 F PWM: Randomized switching frequency PWM

Table 5. Comparison of radial force at slip=0.0.

Frequency	100Hz	400Hz	f_c	$2f_c$
Line	0.815	0.0467	--	--
PWM	0.813	0.0455	0.00560	0.00263
P PWM	0.821	0.0455	0.00480	0.00171
F PWM	0.815	0.0454	0.00516	0.00142

Table 6. Comparison of radial force at slip=0.05.

3.7. Discussions

The steady state characteristics of the induction motor can be calculated by the 2D FEM considering the modified conductivity in the rotor slot by (12) and the leakage inductance of stator coil end by (13). However, for the motor with one-slot skewing there is some error in the low speed range, that is, high torque region.

In the section 3.3, it is shown that the space variation of the radial force is approximately flat in the teeth and becomes a small value at the positions where the rotor slot exists. The radial force at one tooth is bigger than that at the other two teeth, when the stator winding is distributed in three slots as shown in Fig. 14. It is also shown that the radial force has a fundamental frequency of 2 times the line frequency of 50Hz, because this motor is two pole pairs machine. Moreover, some frequencies of the radial force are obtained by considering the stator magnet-motive force and the rotor slot permeance.

In the section 3.4, when the motor is driven by the PWM inverter, the current and torque contain the component of the carrier frequency as well known. As a result, the waveform of the radial force also includes small noise. The Fourier analysis shows that the fundamental component is almost same as that driven by line source, and that the amplitude around 5 kHz, that is, carrier frequency is bigger than that of the line source as shown in Figs. 22 and 26.

In the section 3.5, the measurement of vibration velocity shows that there are vibration at around natural frequency and some frequencies corresponding to the radial force. However, there are the other frequencies corresponding to the harmonics of line frequency and the frequency produce by the eccentricity of the rotor

In the section 3.6, the effect of the randomized PWM inverter on the radial force is calculated. Two types of random PWM method, namely, a randomized pulse position PWM and a randomized switching frequency PWM are taken into account.

However, the time spectrum shown in Figs 29 and 30 are approximately the same as that under line source, except for the reduction of radial forces at two times carrier frequency. The calculation was carried out for about five cycles of the fundamental frequency. If a very long period is calculated, the reduction of radial force at the carrier frequency becomes larger.

4. Conclusion

The natural frequencies of the motor can be estimated by considering the equivalent Young's modulus of the stator windings. For example, the lowest measured and calculated natural frequencies are 1,325 and 1,369 Hz for the stator core only, and are 637 and 587 Hz for the stator core with winding. They agree well with each other.

The steady state characteristics of the induction motor can be calculated by the 2D FEM considering the modified conductivity in the rotor slot and the leakage inductance of stator coil end. Using this simulation model, the radial force of the induction motor fed by the line source has been analyzed. It is shown that the frequencies are explained by the product of the fundamental stator MMF and the rotor slot permeance, and that the radial force is different at each tooth because of the distributed stator winding.

When the motor is driven by the PWM inverter, the fundamental component of radial force is almost same as that driven by line source and the amplitude around the carrier frequency is bigger than that of the line source. Moreover, the effect of the randomized PWM inverter on the radial force is calculated. The radial forces at two times carrier frequency can be reduced by using the randomized pulse position PWM or by the randomized switching frequency PWM.

Author details

Takeo Ishikawa
Gunma University, Japan

5. References

- F. Ishibashi, K. Kamimoto, S. Noda, and K. Itomi, Small induction motor noise calculation, *IEEE Trans. on Energy Conversion*, vol.18, no.3 pp.357-361, 2003.
- K. Shiohata, K. Nemoto, Y. Nagawa, S. Sakamoto, T. Kobayashi, M. Itou, and H. Koharagi, A method for analyzing electromagnetic-force-induced vibration and noise analysis, (in Japanese) *Trans. IEE Japan*, vol.118-D, no.11 pp.1301-1307, 1998.
- D. M. Munoz, J. C. S. Lai, Acoustic noise prediction in a vector controlled induction machine, 2003 IEEE international Electric Machines and Drives Conference, pp.104-110, 2003.
- Technical Report on Computational method of Electromagnetics for Virtual Engineering of Rotating Machinery, (in Japanese) *IEE Japan*, vol. 776, March, 2000.
- D. Mori and T. Ishikawa, Force and Vibration Analysis of Induction Motors, *IEEE Transactions on Magnetics*, Vol. 41, No.5, pp. 1948-1951, 2005.
- D. Mori and T. Ishikawa, Force and Vibration Analysis of a PWM Inverter-Fed Induction Motor, *The 2005 International Power Electronics Conference*, pp.644-650, Niigata, 2005
- T. Horii, *Electrical Machines Outline*, Corona, publishing Co., Ltd., 1978

- K. Yamasaki, Modification of 2D Nonlinear time-stepping analysis by limited 3D analysis for induction machines, *IEEE Trans. on Magnetics*, vol.33, no.22, 1997
- H. Kometani, S. Sakabe, and N.Nakanishi, 3-D Electromagnetic analysis of a cage induction motor with rotor skew, *IEEE Trans. on Energy Conversion*, vol.11, no.2, 1996
- A. M. Trzynadlowski, F. Blaabjerg, J. K. Pedersen, R. L. Kirlin, and S. Legowski, Random Pulse Width Modulation Techniques for Converter-Fed Drive Systems - A Review, *IEEE Trans. on Industry Applications*, vol. 30, No.5, pp.1166-1175, 1994.
- K. Itori, S. Noda, F. Ishibashi, and H. Yamawaki, Young's modulus of windings on finite element method for natural frequency analysis of stator core in induction motor, (in Japanese) *Trans. of the Japan Society of Mechanical Engineers, Series C*, vol. 68, no.669, pp.1-6, 2002.